*Progress In Electromagnetics Research C, Vol. 135, 131–144, 2023*

# A Multiband Flexible Wideband CPW Wearable Slot Antenna for Biomedical and IoT Applications

**Nageswara R. Regulagadda[1, *] and Uppalapati Venkata Ratna Kumari[2]**

**Abstract**—This paper presents a multiband flexible wideband coplanar waveguide (CPW) wearable slot antenna for biomedical and Internet of Things (IoT) applications. The proposed antenna comprises an elliptical patch with a slot designed on top of a thin and flexible polyimide substrate of thickness 0.1 mm. CPW feeding with slotting on the ground and a protruding microstrip from the ground on one side of the patch is used to have resonance at multi-frequencies for the proposed antenna design. The measured results show that the developed antenna resonates at 2.81 GHz with an impedance bandwidth of 0.8 GHz (2.23–3.2 GHz) and at 4.43 GHz, 5.96 GHz, and 9.38 GHz with an impedance bandwidth of 6.7 GHz (3.5–10.3 GHz). The proposed antenna is simple and portable to mount on any part of the human body and obtains justified specific absorption rate (SAR) values. The prototype of the suggested antenna underwent the fabrication process. A comparison of the antenna parameters was carried out, and there was a reasonable correlation between the simulation and measured results. The proposed antenna is a good contender for Wireless Body Area Networks (WBANs) and IoT applications.

## 1. INTRODUCTION

The goal of wearable antenna technology that involves embedding antennas in clothing or placing them on the human body is to improve communication and navigation. Wearable antennas are essential for Wireless Body Area Networks (WBANs), bio-medical applications like tele-health monitoring systems, and Internet of Things (IoT) devices to make an efficient communication link. Consumer electronics use wearable antennas more and more frequently. Wearable technology enables users to track their essential physiological metrics, monitor their fitness levels, and read text messages more quickly. Wearable technology-enabled devices in the electronic market include implantable devices, smart glasses, smart watches, smart bands for the wrists, and antennas sewn into garments for GPS applications [1].

Wearable antennas should be small and flexible enough to fit on various body areas while remaining undetectable. Microstrip patch antennas and planar inverted-F antennas (PIFAs) are good choices for the design of wearable antennas. Wearable antennas have various types, including printed dipole, microstrip, printed loop, slot, and PIFA antennas for their design [1]. Small, conformable, and flexible wearable antennas are favoured for on-body or on-surface antennas in several applications, such as 5G, IoT, WBAN, and biomedical systems, as they substantially impact the electrical performance of wearable communication systems. In order to serve wearable IoT and biomedical applications and to establish an effective communication link, antennas that exhibit omnidirectional radiation patterns are preferred [2].

A compact, flexible wearable slot antenna for 5 GHz WLAN/WBAN is proposed in [3]. This design uses a rectangular patch with slots on it and a partial ground with a small cut, achieving a good amount of peak gain and wide bandwidth. El Hajj et al. presented the geometry of IIFA fed by a CPW line

*Received 21 May 2023, Accepted 13 July 2023, Scheduled 29 July 2023*
* Corresponding author: Nageswara Rao Regulagadda (nageswararao.regula@gmail.com).
[1] Department of ECE, University College of Engineering JNTU Kakinada, East Godavari, India. [2] University College of Engineering JNTU Kakinada, East Godavari, India.

[4]. This structure led to a bandwidth improvement up to 50% and achieved a small size and dual polarization. Mahmood et al. [5] discussed the flexible antennas with different radii of bent angles and analysed the antenna's performance. It observed that the resonant frequency, SAR, and radiation patterns varied against placing them in the human tissue. De et al. [6] presented a compact, asymmetric CPW-fed, monopole antenna for ultra-wideband (UWB) communication and WBANs. The suggested wearable antenna attained a gain around 6.6 dBi and a fractional bandwidth of 144% at 13.05 GHz by placing a rectangular slit into the ground plane.

Malekpoor [7] obtained increased radiation efficiency, improvement in impedance bandwidth of about 43%, and a good amount of 11 dBi gain by using a broadband planar artificial magnetic conductor (AMC) for the antenna design for X-band operations. The works mentioned in [3, 6, 7] are single-band antennas. If frequency detuning occurs while placing them on human tissue, then the operating band may not serve the target application.

Many research papers have been studied and analysed to understand the design issues, strategies to solve them, and the body effect on wearable antenna design. Considering the problems with wearable antenna designs, a wearable antenna must be durable, small, conformal, and multiband with wide bandwidth to minimize the detuning of resonant frequency for body-worn applications [8]. In this regard, this work focuses on a multiband antenna with wide bandwidth, fabricated on a flexible substrate material, and the same is obtained with the use of a slotted patch with CPW feeding. Slots on the patch and ground with an extension of the ground on the edge of the patch are used in view of achieving multiband behaviour for the suggested antenna with promising impedance matching. The CPW feeding method is used to attain a broad bandwidth for the proposed antenna [9].

The contribution of this work can be summarized as follows:

- An antenna is designed for wearable applications using flexible polyimide of 0.1 mm thickness as a substrate material.
- The slotted antenna with CPW feed ensures a good amount of size reduction, increased electrical length without much increase in antenna dimensions, and resonates at two ISM bands (2.45 GHz & 5.8 GHz), and the two are 4.43 GHz and 9.38 GHz.
- For all the operating bands, the antenna achieves wide bandwidth and UWB characteristics for higher bands (3.56 GHz–10.3 GHz).
- The SAR values on human phantoms are well below the standard value, ensuring the bio-compatibility of the antenna design.

The work presented in this paper is divided into five sections. Section 1 deals with the introduction to wearable devices and their demand in the present electronic market, the challenges of wearable antenna design, some works on wearable antenna design from the literature, and the motivation for the proposed work. Section 2 explores the design steps involved in obtaining the proposed antenna design. Section 3 mentions the details about the parametric study of the proposed antenna. Section 4 discusses the computed and measured results of various performance metrics of an antenna and their comparison details, followed by the conclusion of the proposed work.

## 2. ANTENNA DESIGN

This research study suggests a wearable, portable antenna that resonates across several frequency bands. The substrate and conducting materials in the proposed antenna design are made of 0.1 mm thick polyimide and 0.035 mm thick copper sheet, respectively. This design uses the CPW feeding technique for the excitation. The polyamide material has excellent impedance matching with a dielectric constant value of 3.5 and a dielectric loss tangent of 0.008. It is ideal for flexible substrates because of its low dielectric constant, excellent mechanical strength, thermal stability, and high chemical resistance compared to paper [10]. The fundamental equation used to build the suggested antenna is,

$$f_L(\text{GHz}) = \frac{c}{\lambda} = \frac{7.2}{L + r + p} \tag{1}$$

where $f_L$ is the lower end point of the impedance bandwidth; '$r$' and '$L$' are the radius and length of cylindrical monopole antenna, respectively; and '$p$' is the gap between the radiating patch and the

ground plane. The dimensions of $L$ and $r$ in Equation (1) can be estimated by equating the area of a cylindrical monopole antenna as

$$2\pi rL = \pi ab \tag{2}$$

Here '$a$' and '$b$' are the dimensions of an elliptical patch antenna. The proposed elliptical patch antenna dimensions are chosen to make areas of the elliptical and cylindrical monopole antennas the same. All the dimensions of suggested antenna are presented in Table 1. The length of the major axis of an elliptical patch ($2a$) is 33 mm, and the minor axis ($2b$) is 28.8 mm. Equation (2) is again modified by changing the feeding method and creating slots on the circular patch to achieve good $S_{11}$ at operating bands.

**Table 1.** Optimum dimensions of the antenna design.

| **Antenna Parameter** | $L1$ | $W1$ | $Lg$ | $Wf$ | $Ls$ | $Ws$ | $a$ | $g$ | $s$ |
|---|---|---|---|---|---|---|---|---|---|
| **Dimensions (mm)** | 52 | 31 | 14.5 | 3.0 | 4.5 | 0.75 | 14.4 | 0.7 | 2.0 |

Suitable slots are introduced at proper locations in the patch and the ground to achieve a reasonable impedance bandwidth with a moderate gain. A small microstrip is protruding from the ground along the length of the substrate to attain multiband behaviour for the proposed antenna. If the microstrip protruding from the ground is on the right of the patch in the positive-$X$ direction, it is antenna 1, and if it is on the left of the $X$ axis, it is antenna 2. The optimum dimensions of the suggested antenna for the targeted operating frequency bands are determined, and Table 1 lists these dimensions. The simulated geometry and the fabricated prototypes of antenna 2 are shown in Figure 1.

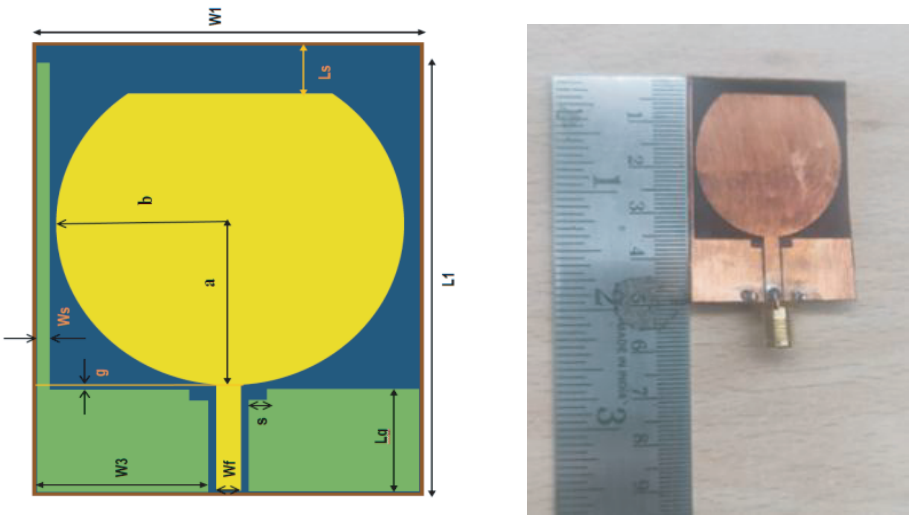


(a) (b)

**Figure 1.** Proposed antenna 2 model. (a) Geometry. (b) Prototype.

### 2.1. Antenna Evolution

The development of the suggested antenna evolved over four stages. In stage 1 (Ant #1), the proposed antenna has a circular patch with a CPW feed. This antenna arrangement resonates at 3.24 GHz and 8.35 GHz with good impedance bandwidth. In the second stage (Ant #2), a small rectangular slot is positioned at the ends of the ground close to the feed point. This arrangement results in two bands only, but there is a shift in the lower band towards the higher frequencies and the upper band frequencies to the lower frequencies with improved bandwidth compared to Ant #1. In stage 3 (Ant #3), a rectangular

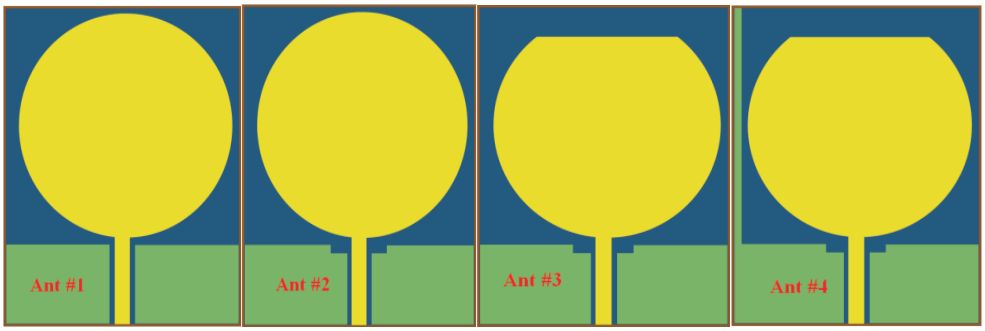


(a)

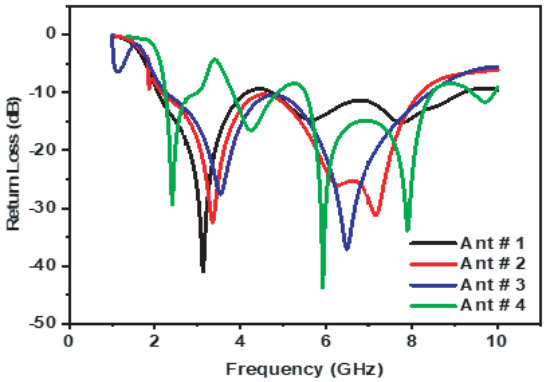


(b)

**Figure 2.** Proposed antenna evolution. (a) Step-by-step evolution of antenna design. (b) Return loss ($S_{11}$) in each stage of the development.

slot is placed on the circular patch, improving return loss ($S_{11}$). Finally, to get the antenna resonated at the desired frequency bands (ISM), Ant #4 is designed by extending a little section of the ground along the length of the substrate. Figure 2(a) represents the evolution of the antenna in four stages. As a result, the developed antenna operates at the resonant frequencies of 2.45 GHz, 4.34 GHz, 5.96 GHz, and 7.96 GHz. Figure 2(b) shows the $S_{11}$ graph of the computed antenna 1 in different phases of its development.

## 3. PARAMETRIC ANALYSES

Various parameters of the antenna are analysed by varying the antenna dimensions, such as the width of the microstrip protruding from the ground, the diameter of the circular disc patch, and the width of a slot on the patch, to achieve good performance for the proposed antenna. Table 2 summarizes the behaviour of the suggested antenna against the variations in the width of the microstrip protruding from the ground on the right of the patch. Figure 3(a) represents the variations in reflection coefficient in terms of $S_{11}$ (dB). Figure 3(b) shows the gain variations (dB), and Figures 3(c) and 3(d) depict the $S_{11}$ and gain graphs against dimensions of a small cut on the ground, respectively.

## 4. SIMULATED AND MEASURED RESULTS

The proposed antenna is constructed and simulated with the calculated dimensions using High-Frequency Structure Simulator (HFSS) software, and the output parameters are examined to confirm the design. The final design of the suggested antenna is obtained in 4 steps, antenna #1, antenna #2, antenna #3, and antenna #4, and in each step, the variations in return loss for the operating frequency

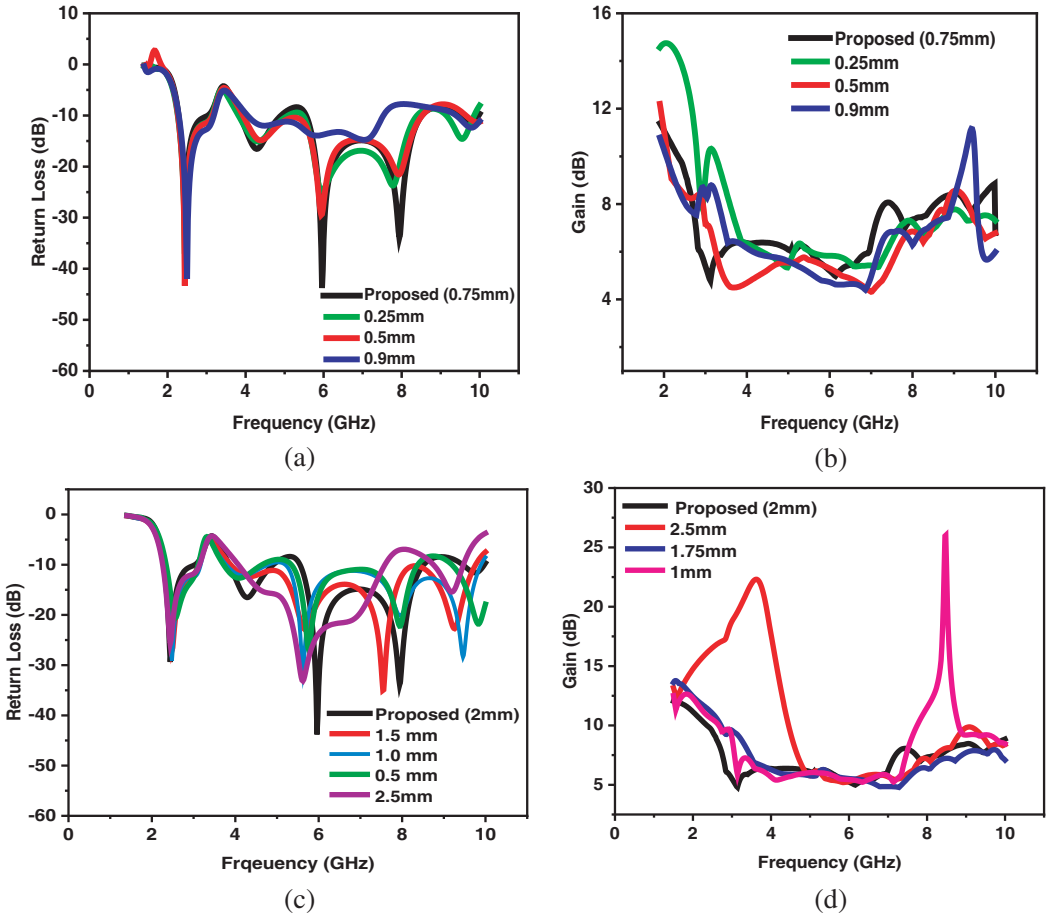


**Figure 3.** Parametric analysis of antenna1. (a) $S_{11}$ graph against different widths of the microstrip protruding from the ground. (b) Variations in gain (dB) against different widths of the microstrip protruding from the ground. (c) Return loss graph against different dimensions of the cut on the ground. (d) Gain graph against different dimensions of the cut on the ground.

range are depicted in Figure 2(b).

Initially, the antenna resonated at two frequency bands. Finally, it resonated at four frequency bands with a good amount of return loss, impedance bandwidth, and good gain for all the frequency bands. The method of slotting was performed to obtain justified output results. The slots on the ground shift the lower frequency band towards higher frequencies and the upper band towards the lower frequencies so that the antenna gets resonated at the targeted ISM (2.4 GHz and 5.8 GHz) bands.

Antenna #1, antenna #2, and antenna #3 resonate at two frequencies only. For antenna #3, the lower band is moved to higher frequencies further with poor return loss, and the higher band is also shifted slightly towards higher frequencies with improved return loss compared to antenna #2. In this case, the proposed antenna does not resonate at the targeted ISM bands. Then, as depicted in Figure 2(a) as antenna #4, the ground is expanded down the length of the substrate with a narrow breadth. Antenna #4 results in resonating at different frequency bands which include the targeted ISM bands 2.4 GHz (2.28–3 GHz) and 5.8 GHz (5.42–8.47 GHz), and the other bands are 4.34 GHz (3.9–4.96 GHz), and 7.94 GHz (5.42–8.47 GHz).

### 4.1. Antenna Simulated Results

The designed antenna is analysed for different performance parameters, and the corresponding simulated results are shown in Figure 4. The summary of the simulated results for all the resonating frequencies is shown in Table 2. Figure 4 displays the simulated co-polarization and cross-polarization graphs at

**Table 2.** The simulated results of proposed antenna 1 for different dimensions of ($Ws$).

| $Ws$ (mm) | Frequency (GHz) | $S_{11}$ (dB) | Bandwidth (GHz) | Gain (dB) |
|---|---|---|---|---|
| 0.25 | 2.44, 4.34, 5.94, 7.78 & 9.46 | −37, −15, −25, −24 & −15 | 0.87, 1.58, 2.92 & 0.71 | 14.76, 6.38, 6.13, 6.14 & 7.63 |
| 0.5 **(Proposed)** | 2.5, 4.58, 5.92, 7.3 & 8.56 | −30, −13, −38, −23 & −18 | 0.97, 4.89, & 0.69 | 10.74, 6.4, 6, 5.9 & 7.44 |
| 0.75 | 2.45, 4.34, 5.96, 7.94 & 9.6 | −43, −15, −29, −21 & −11 | 0.88, 4.59 & 0.55 | 7.2, 4.5, 5.8, 7.6 & 8.2 |

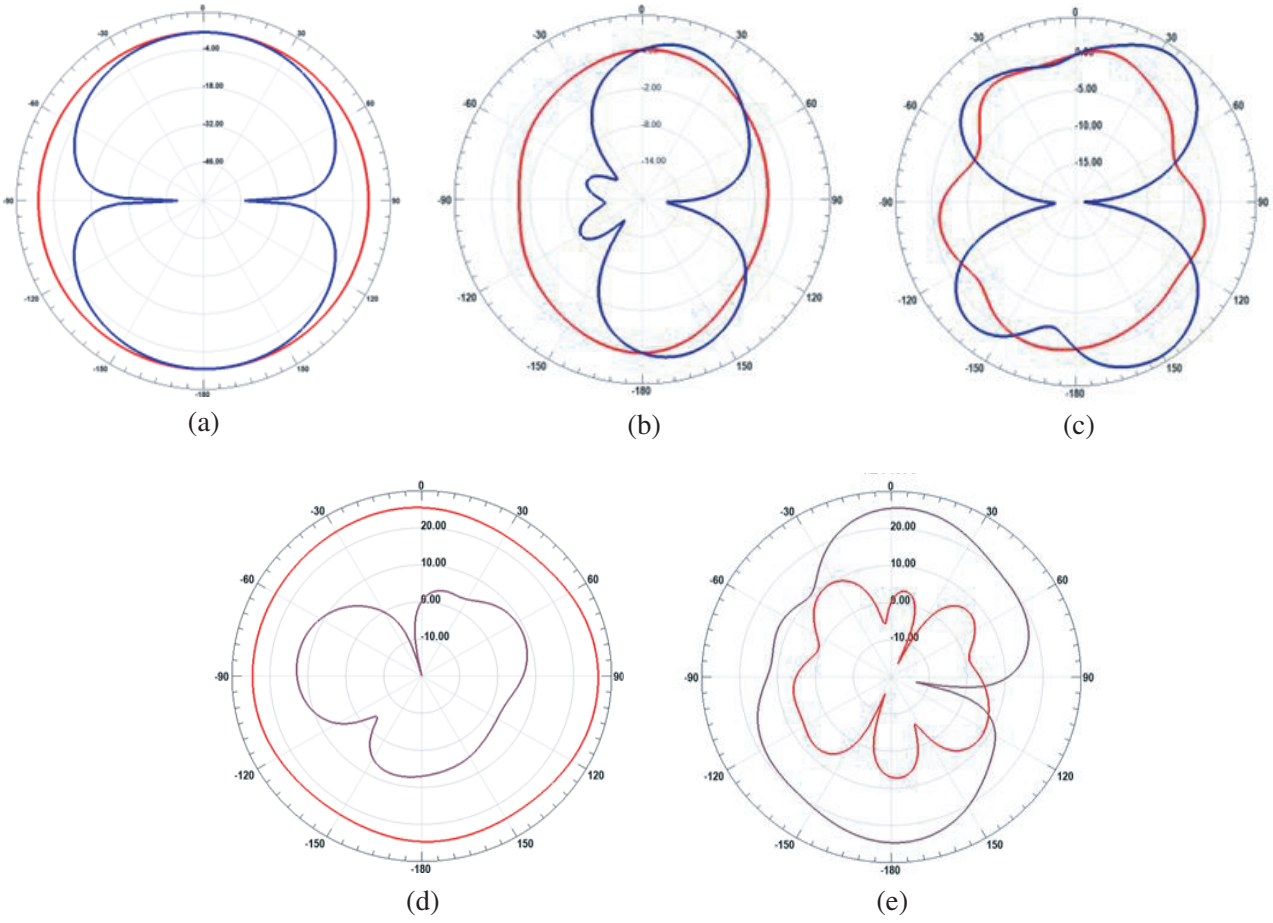


**Figure 4.** The computed results of the designed antenna. (a)–(c) Radiation patterns at 2.45 GHz, 5.96 GHz & 7.94 GHz respectively. (d) & (e) Co-pol and Cross-pol @ $E$-Plane & @ $H$-Plane respectively at 2.4 GHz.

the lower resonating frequency, 2.45 GHz.

### 4.2. Antenna Measured Results

The proposed design is fabricated using Nvis-72 PCB Prototype Machine. The practical results are measured and analysed by test setup ANRISTU Combinational analyzer-MS2037C. The tested results of prototypes are presented in Figures 5(a)–5(c).

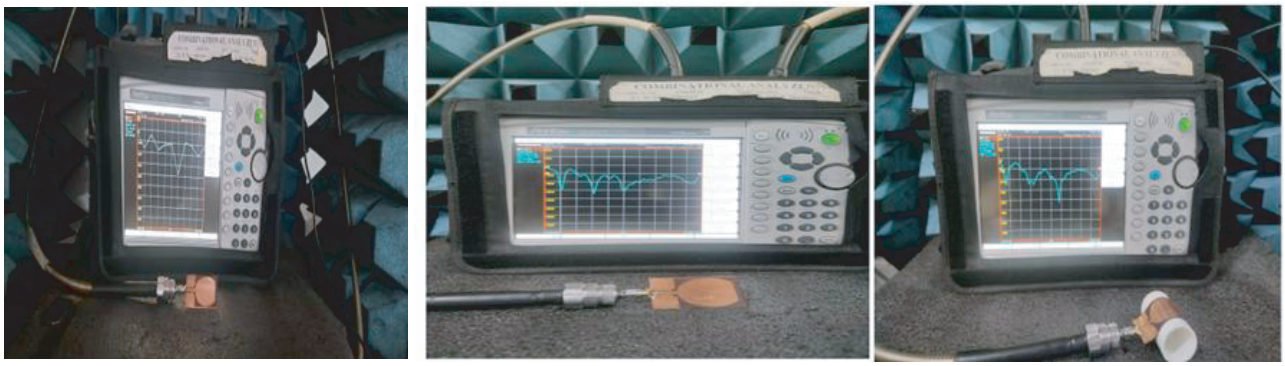

(a) (b) (c)

**Figure 5.** Measured Return Loss $S_{11}$, (a) Antenna 1, (b) Antenna 2, (d) Antenna 2 in bending condition.

### 4.3. Comparison of Computed and Measured Results

To justify the tolerance between the computed and measured results of designed antennas, the comparison results are plotted and presented in Figure 6. Figure 6(a) shows the return loss ($S_{11}$) graph, and Figure 6(b) shows the peak gain (dB) of antenna 1 and antenna 2, respectively. Figure 6(c) presents the computed and measured $E$-plane co-polarization results, and Figure 6(d) shows the $E$-plane cross polarizations results for antenna 1 at 2.4 GHz. The computed and measured results of antenna 2 in bending conditions with a bending radius of 40 mm in free space are depicted in Figure 6(e). Reasonable justification between simulated and measured results is obtained.

The fractional bandwidth (FB) is calculated and compared for all resonating frequencies for antenna 1 and antenna 2. The results are mentioned in the accompanying tables. The FB can be defined as = 2 times $(fH - fL)/(fH + fL)$. Table 3 and Table 4 show the computed and measured results of antenna parameters, including reflection coefficient, bandwidth, and gain for antenna 1 and antenna 2, respectively.

**Table 3.** The output parameters comparison for antenna 1.

| **Frequency (GHz)** | | **$S_{11}$ (dB)** | | **Bandwidth (GHz)** | | **Fractional Bandwidth (%)** | | **Gain (dB)** | |
|---|---|---|---|---|---|---|---|---|---|
| **simu.1** | **msd.1** | **simu.1** | **msds.1** | **simu.1** | **msd.1** | **simu.1** | **msd.1** | **simu.1** | **msd.1** |
| 2.45 | 2.81 | −31.4 | −17 | 2.28–3 | 2.23–3.2 | 27 | 35.7 | 11.43 | 7.18 |
| 4.43 | 4.52 | −16 | −16 | 3.92–5 | 3.5–10.3 | 24 | 98.5 | 5.8 | 4.5 |
| 6.05 | 6.23 | −30 | −39 | 5.5–8.5 | 3.5–10.3 | 42 | 98.5 | 6.1 | 5.8 |
| 7.94 | 8.66 | −35 | −21 | 5.5–8.5 | 3.5–10.3 | 42 | 98.5 | 9.4 | 8.7 |
| 9.9 | | −11 | | 9.8–10 | | 4.6 | | 10 | |

The measured values of the parameters for antenna 1 and antenna 2 and the details are presented in Table 5. Tables 3, 4, and 5 show that antenna 1 has achieved a decent amount of impedance bandwidth and gain compared to antenna 2. Antenna 1 parameters' divergence between measured and simulated values is significant. Thus, antenna 2 is regarded as the final proposed design since it demonstrates the justified agreement between the computed and measured findings for the two ISM bands, focused on in this study.

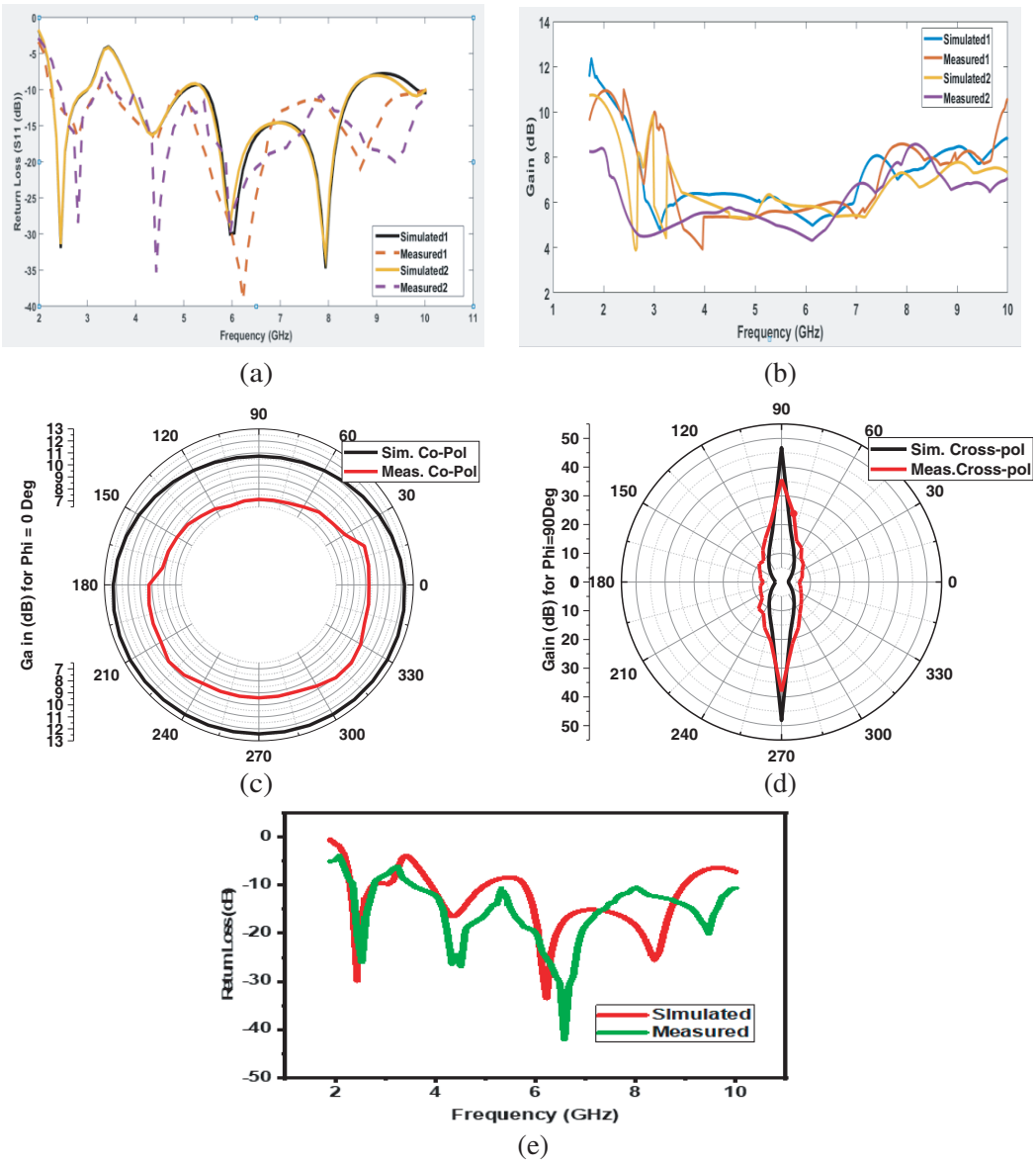


**Figure 6.** The results comparison of proposed antenna antenna 1 and antenna 2. (a) Return Loss of antenna 1 and antenna 2. (b) Gain antenna1 and antenna 2. (c) Co-Pol radiation of antenna 2. (d) Cross-Pol radiation of antenna 2. (e) $S_{11}$ graph when antenna 2 is bent.

### 4.4. Flexibility of the Proposed Antenna

Various conductive and dielectric materials have been used in wearable antenna design. Hence, it is necessary to select these materials so that they can withstand mechanical deformations, including bending, twisting, and wrapping. The suggested antenna structure is bent in the $X$ direction with different bent radii, and the respective $S_{11}$ is depicted in Figure 7. It is observed from Figure 7(c) that there is not much deviation in unbent $S_{11}$ from that of bent $S_{11}$ of antenna 1. The computed and measured results of antenna 2 for bent and unbent states are compared, and the findings are shown in Table 6. Table 7 displays antenna 2's $S_{11}$ graph for a bending radius of 40 mm. It is evident that the computed and measured $S_{11}$ are justified, particularly for ISM band frequencies, as well as that of antenna 2 in its unbent condition.

**Table 4.** The output parameters comparison for antenna 2.

| **Frequency (GHz)** | | **$S_{11}$ (dB)** | | **Bandwidth (GHz)** | | **Fractional Bandwidth (%)** | | **Gain (dB)** | |
|---|---|---|---|---|---|---|---|---|---|
| **simu.2** | **msd.2** | **simu.2** | **msd2** | **simu.2** | **msd.2** | **sim.2** | **msd.2** | **sim.2** | **Msd.2** |
| 2.45 | 2.81 | −31.33 | −28.5 | 2.28–3 | 2.4–3.2 | 27 | 28.5 | 7.2 | 5.3 |
| 4.34 | 4.43 | −17.14 | −35 | 3.9–4.96 | 3.56–10.3 | 24 | 97 | 4.5 | 5.7 |
| 5.96 | 5.96 | −30.67 | −30 | 5.42–8.47 | 3.56–10.3 | 44 | 97 | 5.8 | 4.5 |
| 7.94 | 9.38 | −33.10 | -20 | 5.42–8.47 | 3.56–10.3 | 44 | 97 | 7.6 | 6.8 |
| 9.7 | | −12 | | 9.6–10.3 | | 3.5 | | 8.2 | |

**Table 5.** The measured return Loss & bandwidth of the antenna 1 and antenna 2 at resonant frequencies.

| **Frequency (GHz)** | | **Return Loss $S_{11}$ (dB)** | | **Bandwidth (MHz)** | | **Fractional Bandwidth (%)** | |
|---|---|---|---|---|---|---|---|
| **Antenna 1** | **Antenna 2** | **Antenna 1** | **Antenna 2** | **Antenna 1** | **Antenna 2** | **Antenna 1** | **Antenna 2** |
| 2.81 | 2.81 | −17 | −28.5 | 300 | 800 | 35.7 | 28.5 |
| 4.52 | 4.43 | −16 | −35 | 6800 | 6740 | 98.5 | 97 |
| 6.23 | 5.96 | −39 | −30 | 6800 | 6740 | 98.5 | 97 |
| 8.66 | 9.38 | −21 | −20 | 6800 | 6740 | 98.5 | 97 |

**Table 6.** Comparison of the antenna-2 parameters in unbent and bending conditions.

| **Frequency (GHz)** | | | | **$S_{11}$ (dB)** | | | | **Bandwidth (MHz)** | | | |
|---|---|---|---|---|---|---|---|---|---|---|---|
| **Simul.** | | **Meas.** | | **Simul.** | | **Meas.** | | **Simul.** | | **Meas.** | |
| Unbent | Bent | Unbent | Bent | Unbent | Bent | Unbent | Bent | Unbent | Bent | Unbent | Bent |
| 2.48 | 2.42 | 2.5 | −31 | 2.85 | −39 | −16 | −23 | 860 | 840 | 320 | 550 |
| 4.37 | 4.28 | 4.4 | −18 | 4.45 | −16 | −17 | −22 | 5490 | 1560 | 6700 | 2040 |
| 6.16 | 5.82 | 6.7 | −16 | 6 | −45 | −40 | −41 | 5490 | 3120 | 6700 | 5000 |
| 8.42 | 8.2 | 9.3 | −23 | 9.4 | −31 | −21 | −20 | 5490 | 4320 | 6700 | 5000 |

**Table 7.** The antenna 2's parameters, when bent with a radius of 40 mm.

| **Frequency (GHz)** | | **$S_{11}$ (dB)** | | **Bandwidth (MHz)** | |
|---|---|---|---|---|---|
| **Simul.** | **Meas.** | **Simul.** | **Meas.** | **Simul.** | **Meas.** |
| 2.48 | 2.55 | −30 | −26 | 470 | 500 |
| 4.37 | 4.4 | −17 | −26 | 1300 | 2400 |
| 6.16 | 6.65 | −33 | −42 | 3180 | 5000 |
| 8.42 | 9.34 | −25 | −20 | 3180 | 5000 |

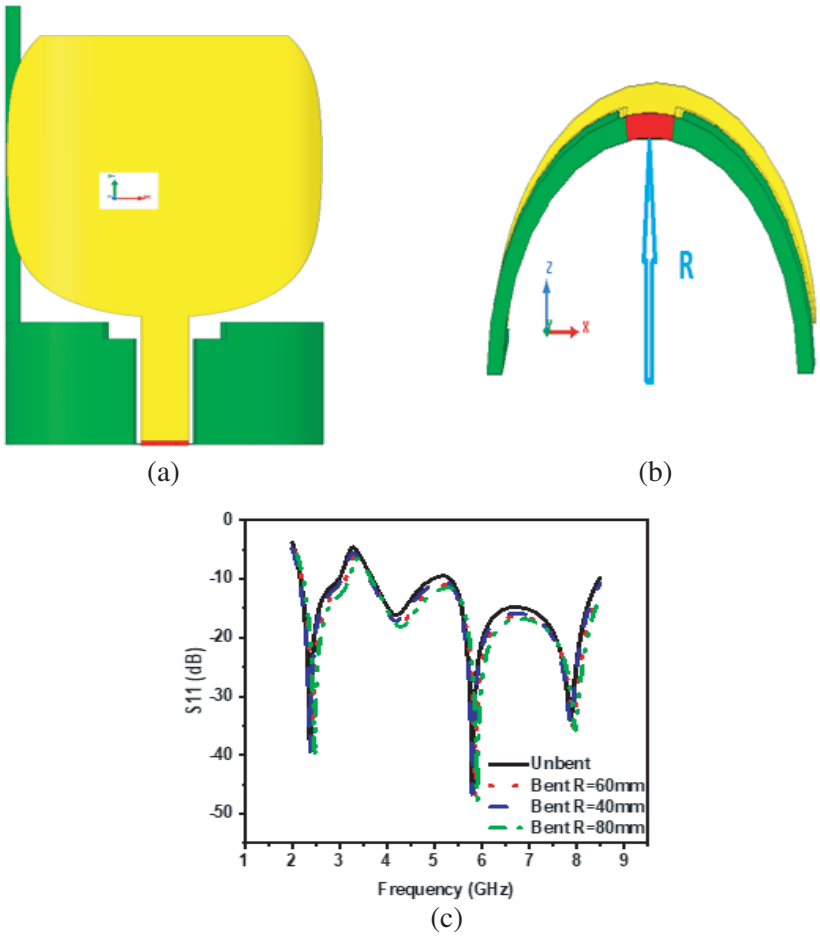


**Figure 7.** The suggested antenna's flexibility test: (a) Antenna in bending condition; (b) Various bending radii; (c) $S_{11}$ comparison graph with different bent angles.

### 4.5. Human Loading

The effect of human loading on the proposed antenna in terms of return loss and radiation pattern is analyzed by designing a three layer human tissue model [3]. The three layer (skin, fat and muscle) human tissue model is created in HFSS tool and is shown in Figure 8. Figure 8(a) shows the rectangular shaped human tissue model. Figure 8(b) depicts the vertical cut view of cylinder-shaped three layer human tissue model, and Figure 8(c) indicates the return loss graph for various conditions. Figure 8(d) highlights the radiation pattern of the proposed antenna in free space in unbent condition and when antenna is bent on human tissue model at 5.8 GHz ISM band.

### 4.6. Specific Absorption Rate

The amount of electromagnetic wave diffusion in bodily tissues can be calculated using the antenna's Specific Absorption Rate (SAR) and is measured in Watts (W)/kilogram (kg). The antenna performance can also depend on the diverse and lossy characteristics of the human tissue. As shown in Figure 9, the antenna's effectiveness is assessed for On-Body integration through simulation. The suggested antenna is placed on the human head and the human arm phantom models, and the respective simulated maximum SAR is calculated as 0.01394 W/kg and 1.2931 W/kg using the HFSS simulation tool. The SAR values thus obtained are far below the standard values.

The suggested antenna has been compared with the existing works designed for the 2.4 GHz ISM band in the literature to find its suitability for biomedical and IoT applications. The comparison details

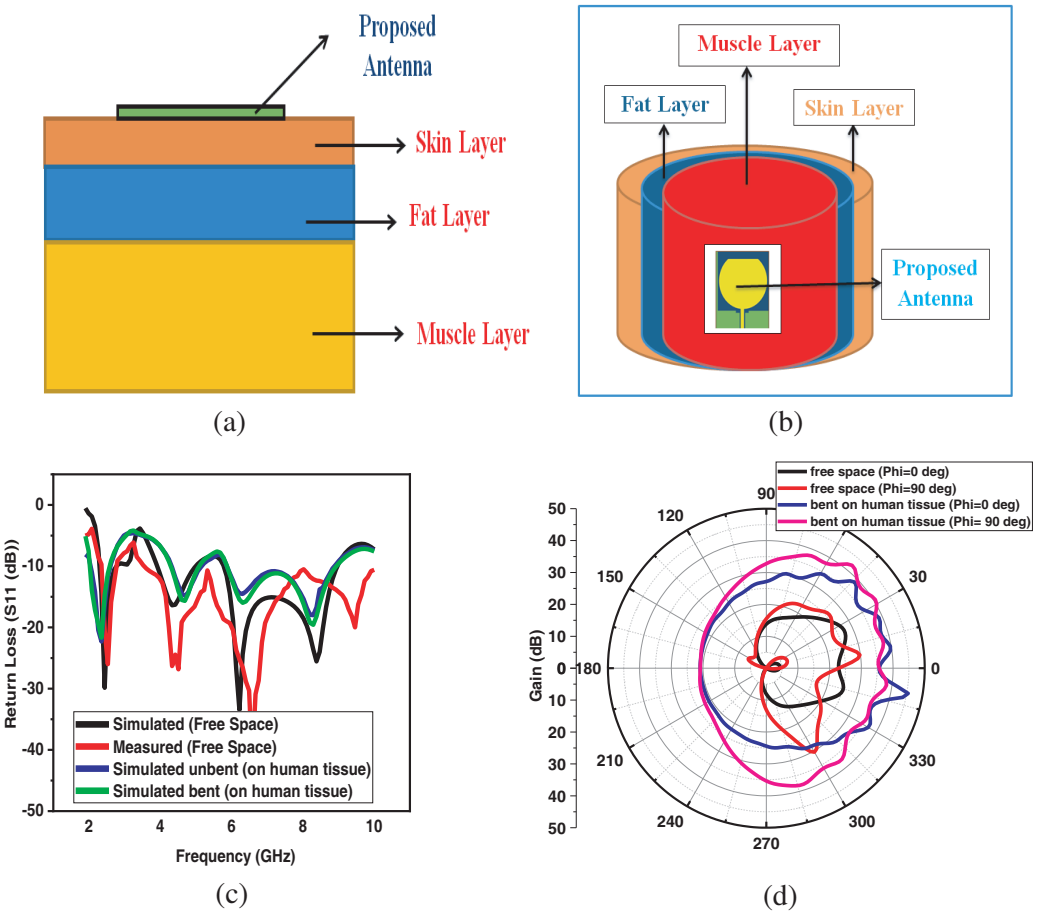


**Figure 8.** Proposed antenna with human loading (a) in unbent condition, (b) in bent condition, (c) return loss ($S_{11}$) in different environments. (d) Radiation pattern in free space unbent condition and when bent on human tissue.

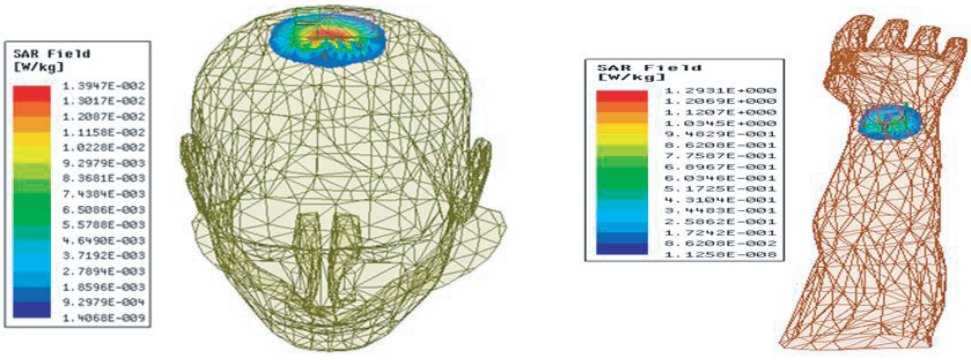


**Figure 9.** The simulated SAR (a) on human head phantom, (b) on human arm phantom.

are presented in Table 8. The suggested antenna has high impedance bandwidth and moderate gain at ISM 2.45 GHz.

Antenna 2 has been compared with the existing multiband antennas in the literature. The comparison is made on the parameters like substrate materials, type of miniaturization method, antenna size, gain, and SAR values. The particulars are presented in Table 9. It is clear from Table 9 that

**Table 8.** Comparison of the proposed work with the literature at 2.4 GHz ISM band applications.

| Reference | Antenna size ($mm^3$) | Bandwidth (GHz) | Fractional Bandwidth (%) | Gain (dBi) | SAR (w/kg) |
|---|---|---|---|---|---|
| [11] | $60 \times 60 \times 2.4$ | 2.3–2.5 | 8.3 | 6.55 | 0.055 |
| [12] | $81 \times 81 \times 4$ | 2.28–2.64 | 14.7 | 7.3 | 0.554 |
| [13] | $39 \times 39 \times 0.503$ | 2.36–2.55 | 7.75 | 2.06 | 1.56 |
| [14] | $8.14 \times 8.14 \times 1$ | 2.36–2.47 | 4.5 | 8 | NA |
| **Proposed*** | $\mathbf{31 \times 52 \times 0.1}$ | **2.4–3.2** | **28.5** | **5.3** | **0.0139** |

**Table 9.** Comparison of the multiband nature of the designed antenna with the literature.

| Reference | Antenna size ($mm^3$) | Dielectric (material) | Fractional Bandwidth (%) | Gain (dBi) | SAR (w/kg) |
|---|---|---|---|---|---|
| [15] | $60 \times 60 \times 1.17$ | Denim | 0.09, 0.19, 2.9 & 3.8 | −0.8, −2.8, −1 & 3 | —- |
| [16] | $24 \times 19 \times 1.53$ | Polyamide | 5.8, 6.3 & 6.6 | 3.73 @ 5.6 GHz | 0.37, 0.45 & 1.27 |
| [17] | $90 \times 78 \times 3$ | Felt | 2.5, 5.7, 42 & 5.2 | 1.75, 3, 6 & 3 | —- |
| [18] | $60 \times 60 \times 3.6$ | TLY-5/Felt | 4.4, 4 & 6 | 6.2, 7.8 & 5.8 | 0.13, 0.09 & 0.09 |
| [19] | 20 mm radius | Leather | 13, 13.95 & 10.84 | 2.3, 2.7 & 3 | 0.93, 0.89 & 0.97 |
| This work | $52 \times 31 \times 0.1$ | Polyimide | 28.5, 97, 97 & 97 | 5.3, 5.7, 4.5 & 6.8 | 1.29 & 0.0139 |

antenna 2 presented in this work has high impedance bandwidth, moderate gain, moderate size, and low profile for all the operating frequency bands.

## 5. CONCLUSIONS

Wearable electronics, which may be attached to the human body or placed near the human tissue, are helpful in tracking the body's vital signs and identifying and monitoring health conditions. For ISM band biomedical and IoT applications, a wearable, adaptable, portable antenna that resonates over several bands is suggested. A low-profile, circular slot antenna with a CPW feed is constructed with dimensions of $52 \times 31\,mm^2$. It is mounted on a thin, flexible polyimide substrate (0.1 mm). At the resonant frequencies 2.45 GHz, 4.34 GHz, 5.96 GHz, and 7.94 GHz, antenna performance metrics such as reflection coefficient in terms of $S_{11}$, gain, and impedance bandwidth are obtained. The designed antenna's behaviour is examined under bending situations with various bending radii and in different environments like in free space and on three layer human tissue model. The proposed antenna's SAR value has been computed using phantom models of a human head and an arm, and it is found that the SAR value is below IEEE standards. Thus, a strong argument for its use in biomedical and IoT applications may be found by examining the comparison graphs drawn between the computed and measured outcomes.

## 6. ORCID ID

Nageswara Rao RiD https://orcid.org/0000-0002-8223-8164.

## REFERENCES

1. Sabban, A., "Small new wearable antennas for IOT, medical, and sports applications," *13th European Conference on Antennas and Propagation (EuCAP)*, 1–5, Krakow, Poland, 2019.
2. Khan, U. R., J. A. Sheikh, A. Junaid, R. Amin, S. Ashraf, and S. Ahmed, "Design of a compact hybrid Moore's fractal inspired wearable antenna for IoT enabled bio-telemetry in diagnostic health monitoring system," *IEEE Access*, Vol. 10, 116129–116140, 2022, doi: 10.1109/ACCESS.2022.3219442.
3. Regulagadda, N. R. and U. Venkata Ratna Kumari, "A low profile wearable slot antenna with partial ground for 5 GHz WLAN/WBAN applications," *Progress In Electromagnetics Research C*, Vol. 128, 183–193, 2023.
4. El Hajj, W., C. Person, and J. Wiart, "A novel investigation of a broadband integrated inverted-F antenna design; Application for wearable antenna," *IEEE Transactions on Antennas and Propagation*, Vol. 62, No. 7, 3843–3846, July 2014, doi: 10.1109/TAP.2014.2318061.
5. Mahmood, S. N., A. J. Ishak, T. Saeidi, H. Alsariera, S. Alani, A. Ismail, and A. C. Soh, "Recent advances in wearable antenna technologies: A review," *Progress In Electromagnetics Research B*, Vol. 89, 1–27, 2020.
6. De, A., B. Roy, A. Bhattacharya, and A. K. Bhattachaqee, "Bandwidth-enhanced ultra-wide band wearable textile antenna for various WBAN and Internet of Things (IoT) applications," *Radio Science*, Vol. 56, No. 11, 1–16, Nov. 2021, doi: 10.1029/2021RS007315.
7. Malekpoor, H., "Broadband printed tapered slot antenna fed by CPW fulfilled with planar artificial magnetic conductor for X-band operation," *Advanced Electromagnetics*, Vol. 12, No. 1, 1–10, 2023, https://doi.org/10.7716/aem.v12i1.2087.
8. Khan, U. R., J. A. Sheikh, A. Junaid, R. Amin, S. Ashraf, and S. Ahmed, "Design of a compact hybrid Moore's fractal inspired wearable antenna for IoT enabled bio-telemetry in diagnostic health monitoring system," *IEEE Access*, Vol. 10, 116129–116140, 2022, doi: 10.1109/ACCESS.2022.3219442.
9. Sinha, S., B. Rana, C. K. Ghosh, and S. K. Parui, "A CPW-fed microstrip antenna for WLAN application," *Procedia Technology*, Vol. 4, 417–420, 2012.
10. Khaleel, H. R., H. M. Al-Rizzo, D. G. Rucker, and S. Mohan, "A compact polyimide-based UWB antenna for flexible electronics," *IEEE Antennas and Wireless Propagation Letters*, Vol. 11, 564–567, 2012.
11. Ashyap, A. Y. I., Z. Zainal Abidin, S. H. Dahlan, H. A. Majid, M. R. Kamarudin, A. Alomainy, et al., "Highly efficient wearable CPW antenna enabled by EBG-FSS structure for medical body area network applications," *IEEE Access*, Vol. 6, 77529–77541, 2018.
12. Gao, G.-P., B. Hu, S.-F. Wang, and C. Yang, "Wearable circular ring slot antenna with EBG structure for wireless body area network," *IEEE Antennas and Wireless Propagation Letters*, Vol. 17, No. 3, 434–437, Mar. 2018.
13. Arif, A., M. Zubair, M. Ali, M. U. Khan, and M. Q. Mehmood, "A compact low-profile fractal antenna for wearable on-body WBAN applications," *IEEE Antennas and Wireless Propagation Letters*, Vol. 18, No. 5, 981–985, May 2019.
14. Mohan, C. and S. E. Florence, "Miniaturised triangular microstrip antenna with metamaterials for wireless sensor node applications," *IETE J. Res.*, 1–6, Jul. 2019.
15. Li, H., J. Du, X.-X. Yang, and S. Gao, "Low-profile all-textile multiband microstrip circular patch antenna for WBAN applications," *IEEE Antennas and Wireless Propagation Letters*, Vol. 21, No. 4, 779–783, Apr. 2022, doi: 10.1109/LAWP.2022.3146435.

16. Sreelakshmi, K., G. S. Rao, and M. N. V. S. S. Kumar, "A compact grounded asymmetric coplanar strip-fed flexible multiband reconfigurable antenna for wireless applications," *IEEE Access*, Vol. 8, 194497–194507, 2020, doi: 10.1109/ACCESS.2020.3033502.
17. Elias, B. B. Q., P. J. Soh, A. A. Al-Hadi, R. Joshi, Y. Li, and S. K. Podilchak, "Design of a quad band CPW-fed compact flexible patch antenna for wearable applications," *2020 14th European Conference on Antennas and Propagation (EuCAP)*, 1–5, Copenhagen, Denmark, 2020, doi: 10.23919/EuCAP48036.2020.9135261.
18. Le, T. T., Y.-D. Kim, and T.-Y. Yun, "A triple-band dual-open-ring high-gain high-efficiency antenna for wearable applications," *IEEE Access*, doi: 10.1109/ACCESS.2021.3107605
19. Yang, S., L. Zhang, W. Wang, and Y. Zheng, "Flexible tri-band dual-polarized MIMO belt strap antenna toward wearable applications in intelligent internet of medical things," *IEEE Transactions on Antennas and Propagation*, Vol. 70, No. 1, 2022.